Journal of
Materials Chemistry A

Accepted Manuscript

This article can be cited before page numbers have been issued, to do this please use: D. Prochowicz, M. Franckeviius, A. M. Cielak, S. M. Zakeeruddin, M. Grätzel and J. Lewinski, *J. Mater. Chem. A*, 2015, DOI: 10.1039/C5TA04904K.

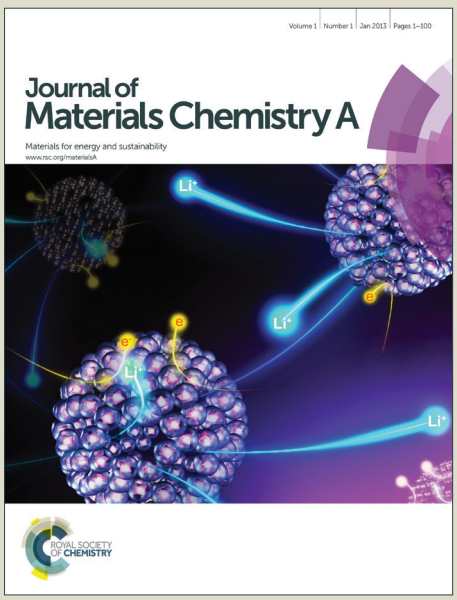

ROYAL SOCIETY OF CHEMISTRY

www.rsc.org/materialsA

View Article Online
DOI: 10.1039/C5TA04904K

Journal Name

ARTICLE

Mechanosynthesis of the Hybrid Perovskite $CH_3NH_3PbI_3$: Characterization and the Corresponding Solar Cell EfficiencyTitle

Received 00th January 20xx,
Accepted 00th January 20xx

DOI: 10.1039/x0xx00000x

www.rsc.org/

D. Prochowicz, [†a] M. Franckevičius, [†bc] A. M. Cieślak,[d] S. M. Zakeeruddin,[b] M. Grätzel[*b] and J. Lewiński [ad]

We present a facile mechanochemical route for the preparation of hybrid $CH_3NH_3PbI_3$ ($MAPbI_3$) perovskite particles with the size of several hundred nanometers for high-efficiency thin-film photovoltaics. Powder X-ray diffraction measurements demonstrates that mechanosynthesis is a suitable strategy to produce highly crystalline $CH_3NH_3PbI_3$ material showing no detectable amounts of the starting CH_3NH_3I and PbI_2 reagents. Thermal stability measurements based on thermogravimetric analysis data of mechanosynthesized perovskite particles, indicated that the as-grounded $MAPbI_3$ are stable up to 300°C with no detectable material loss at lower temperatures. Optical properties of newly synthesized perovskite particles were characterized by applying steady state absorption and fluorescence spectroscopy, which confirmed a direct band band-gap of 1.48eV. Time resolved single photon counting measurements revealed that 70% of charges undergo recombination with a 61 ns lifetime. The solar cell devices made from mechanosynthesized perovskite particles achieved a power conversion efficiency of 9.1% when applying a one step deposition method.

Introduction

Due to their rapid progress in the power conversion efficiencies recently topping at 20.1%,[1] perovskite photovoltaics have become a promising alternative candidate for future power generation from sunlight. The main factors determining the high efficiency of perovskite solar cells are related to their favorable physical properties such as a low band gap and a high extinction coefficient across the entire visible to near infrared region.[2] For efficient charge collection long charge carrier diffusion lengths [3,4] reaching micrometer regime and also high mobilities exceeding tens of square centimetres per voltsecond[5] are very important. However, the presence of defects in perovskite materials can modify the transport and enhance the radiationless decay of mobile charge carriers. Therefore ensuring low concentration of defects is essential for efficient device operation.[6]

In general, preparation methods of perovskite materials play a relevant role on their physical and chemical properties. Their composition, homogeneity, crystallinity, phase purity, morphology, grain size-dispersion, surface area, and many other parameters can be easily altered by simply changing material formation route.[7-9] Therefore sustained efforts have gone into the development of efficient methods for perovskites preparation. The synthesis of $MAPbI_3$ perovskites, where MA stands for the methyl-ammonium cation can be accomplished through a variety of approaches including solvothermal processes and high-temperature solid-state reactions. Some methods have employed grinding a mixture of the appropriate precursors for metalhalide perovskites to achieve more efficient homogenization in the starting mixture.[10,11] It was found that the simple grinding of precursors in a mortar with pestle form a mixture of products including $MAPbI_3$ with significant amounts of unreacted precursors.[11] In such a case, the perovskite purity was increased by further annealing of such "crude" product.

Following our recent reports on a mechano-synthesis as a powerful method for environmentally-friendly, clean and energy-efficient synthesis,[12-15] we report herein an efficient room-temperature mechano-synthesis of the hybrid organic–inorganic perovskite $MAPbI_3$ with well-defined structure and composition. We also demonstrate that such approach applied for preparation of $MAPbI_3$ perovskite material has advantage over a solution based synthetic routes in terms of device performance. To the best our knowledge, this is the first report on the efficient mechano-chemical synthesis of stoichiometric methylammonium lead iodide perovskite powders with its application in photovoltaics.

[a] Faculty of Chemistry, Warsaw University of Technology, Noakowskiego 3, 00-664 Warsaw, Poland.
[b] Laboratory of Photonics and Interfaces, Institute of Chemical Sciences and Engineering, School of Basic Sciences, Ecole Polytechnique Fédérale de Lausanne (EPFL), CH-1015 Lausanne, Switzerland. E-mail: michael.graetzel@epfl.ch
[c] Center for Physical Sciences and Technology, Savanorių Ave. 231, LT-02300 Vilnius, Lithuania.
[d] Institute of Physical Chemistry, Polish Academy of Sciences, Kasprzaka 44/52, 01-224 Warsaw, Poland.
† These authors contributed equally to this work.
Electronic Supplementary Information (ESI) available: [details of any supplementary information available should be included here]. See DOI: 10.1039/x0xx00000x

View Article Online
DOI: 10.1039/C5TA04904K

Results and Discussion

Materials and device preparation

As it was reported by Kanatzidis and cowerkers,[11] simple grinding of MAI and PbI_2 in a mortar with pestle forms a mixture of products with significant amounts of unreacted precursors. We wondered if a more efficient grinding procedure could provide the desired perovskite in high yield and homogeneous form. Indeed, the neat grinding of MAI and PbI_2 (stoichiometric ratio 1:1) in an electric ball mill for 30 min resulted in the formation of polycrystalline methylammonium lead iodide perovskite particles (for experimental details see Supporting Information). The resulting perovskite has been fully characterized using powder X-Ray diffraction (PXRD), thermogravimetric analysis (TGA), steady state absorption and fluorescence spectroscopy and scanning electron microscopy (SEM). The SEM image of one-step perovskite film deposited on mesoporous TiO_2 film is reported earlier[16,17] and we expect no difference to the film prepared by mechanosynthesis method. In the next step, the solar cell device was fabricated by applying one-step deposition method using the mechanochemically synthesized perovskite and its power conversion efficiency was determined.

PXRD data analysis

The powder X-Ray diffraction studies illustrating the formation mechanism of the newly synthesized perovskite particles are presented in Figure 1. The PXRD diagrams of simulated and grounded $MAPbI_3$ perovskite particles are shown in Figure 1 (a) and (b), respectively. The characteristics PXRD spectra of starting precursors, lead iodide and methylammonium iodide, are also presented for comparison in Fig. 1 (c) and (d), respectively. The PXRD analysis of the as prepared perovskite particles reveals well defined patterns which can be attributed to the tetragonal perovskite structure. For comparison, PXRD peak positions of the perovskite particles prepared by mechanosynthesis are also in close agreement to $MAPbI_3$ perovskite materials formed using different fabrication approaches: low temperature vapor-assisted solution process,[18] vacuum deposition[19,20] or solution processed.[21] Only the relative intensities of the PXRD peaks of perovskite materials made by different procedures are slightly different because of the changes in their crystal orientation. Here, one can also observe that the PXRD peaks of mechanosynthesized perovskite crystals are split into two components. This minor displacement in the peak position can be attributed to the formation of additional crystal structure, comprising co-existence of two lattice plains being in close distance, rather than to the formation of additional phases. Moreover, the measured PXRD diagram for mechanosynthesized perovskite (Fig. 1b) ideally match with that of simulated PXRD pattern (Fig. 1a), which was generated based on the lattice parameters with a space group of (I4/mcm)[22] for the tetragonal structure. According to these PXRD measurements, mechanosynthesis allows us to produce highly crystalline $MAPbI_3$ material showing no detectable amounts of the starting MAI and PbI_2 materials.

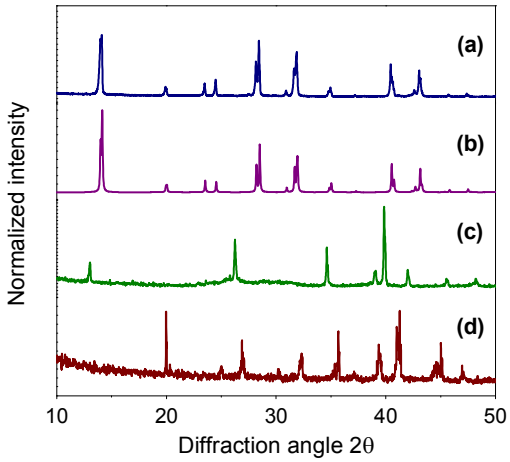

Figure 1 PXRD patterns of: (a) simulated $MAPbI_3$; (b) as grounded $MAPbI_3$; (c) MAI; (d) PbI_2.

Thermal properties

The weight loss as a function of temperature together with its corresponding first derivative of the mechanochemically synthesized $MAPbI_3$ particles measured by thermogravimetric analysis are presented in Figure 2. As is seen, four derivative peaks of different intensities, corresponding to the four mass losses are obtained in the temperature range from 25 to 600°C. Negligibly small loss of a material at 180°C, corresponding to a few percent drop in TGA curve could be assigned to the loss of water. However it is slightly surprising that mechanosynthesis perovskite particles did not show any mass loss below 180 degrees, which was not the case for the solution processed perovskite films, where the first weight loos was obtained in the range between 80 to 130°C attributing it to dehydration of perovskite.[23] Probably mechanosynthesized particles contain a small fraction of more strongly bonded water,[24] which can be released at slightly higher temperatures comparing to the water which is just adsorbed on the surface. Similar temperature value for the release of strongly bounded water molecules were previously reported from various compounds[25,26]. Whereas, a first significant mass loss appears at around 250°C and reaches maximum rate at 350°C. According to the previous data,[23] the mass loss in this temperature interval can be attributed to the loss of HI, while the loss appearing from 350 to 400 degrees may be attributed to the sublimation of the amine constituent. It follows, that the decrease in weight, occurring in two steps in the range from 250 to 400 degrees, consists only of the loss of methylammonium iodide. In agreement with the experimentally obtained data it constitutes about 25% of total weight of $MAPbI_3$. Finally, the last step which starts at around 450°C in TGA curve is due to thermal decomposition of the lead iodide which is completed at 600°C.

View Article Online
DOI: 10.1039/C5TA04904K

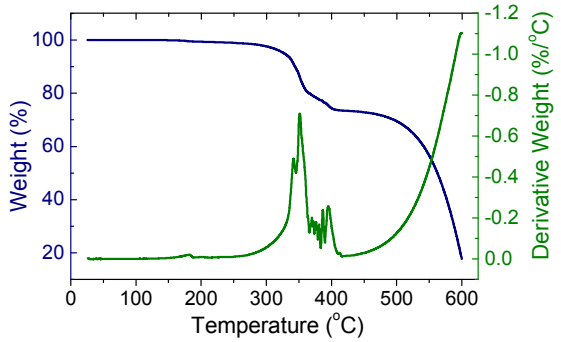

Figure 2 Thermogravimetric analysis traces (blue) and corresponding first derivative (green) as function of the temperature for the as grounded $MAPbI_3$ particles.

Optical properties

Figure 3 presents the UV-vis absorption and fluorescence spectra of methylammonium lead iodide perovskite particles. The measured samples reveal an intense light absorption over the entire UV-visible spectrum (shown in green) with the extrapolated absorption edge corresponding to 1.48 eV band-gap value assuming a direct transition between the edges of valence and conduction bands. The shape of obtained spectrum is typical of methylammonium lead iodide perovskites, however the somewhat lower band gap, *i.e.* 1.48 vs. the commonly reported 1.55 eV[10,17] may be attributed to the presence of defects produced during the milling process. Probably the small changes in perovskite cristaliinity, which were also observed as a split in PXRD spectra, could be the main parameter that is contributing to slightly lowering band gap position of the mechanosynthesis perovskite particles. Photoluminescence spectra of the as-grounded $MAPbI_3$ shows a strong exciton emission at 1.57 eV (Figure 3). To gain better understanding on the charge recombination mechanism in newly synthesized perovskite particles we have performed excited-state photoluminescence lifetime measurements using time correlated single photon counting spectroscopy. The insert in Fig. 3 shows the photoluminescence decay of mechanosynthesis perovskite particles, measured in air at 1.57 eV upon sample excitation at 3.05 eV. The fluorescence decay kinetic was fit by the sum of two exponentials width lifetime of 4.5 ns and 61 ns. The fast decay fraction is 30% and the slower decay accounts for the remaining 70%.

SEM analysis

The low-magnification SEM images of the as-grounded $MAPbI_3$ particles show that the particles exhibit average diameters of about 250-450 nm (Figure SI 1 (a) and (b)). As shown in Fig. SI 1 (b), the presence of individual particles is not dominating and the formation of larger aggregated clusters is also probable when applying this synthesis method. The shape of formed perovskite particles is rarely hexagonal but mainly irregular and also independent on their size. Probably the geometrical parameters mainly depends on grinding conditions rather than on self-assembly of perovskite crystals.

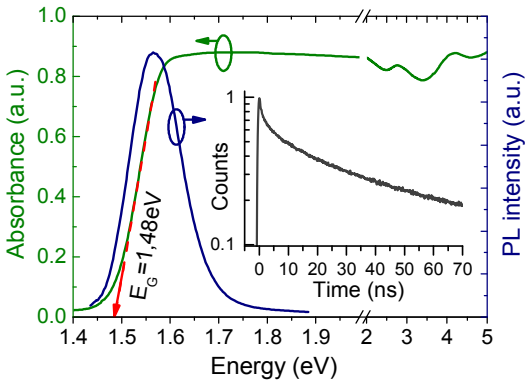

Figure 3 Steady state absorption (green) and photoluminescence (blue) spectra of as-grounded $MAPbI_3$ measured at room temperature. Fluorescence decay measured at fluorescence maximum upon sample excitation at 3.05 eV is presented in the insert.

Photovoltaic performance

Having the newly synthesized perovskite in hand, designate further as $MAPbI_3$[m], we attempted to investigate its behavior as the light-absorbing material to fabricate solution-processed solid-state photovoltaic device. For comparison of photovoltaic performance, the reference material $MAPbI_3$ (designate as $MAPbI_3$[s]) was synthesized from direct solvothermal reaction between PbI_2 and MAI (for more details see Experimental Section). Current voltage characteristics of $MAPbI_3$[s] or $MAPbI_3$[m] based devices are shown in Fig. 4a. The photovoltaic parameters of best performing devices are summarized in Table 1. Photovoltaic parameters data of several identical devices are listed in Table SI2. The short circuit photocurrent density (J_{sc}) of the best device fabricated with $MAPbI_3$[m] particles is 1 mA/cm^2 lower than that of the reference device. However, this is overcompensated by a 100 mV higher open circuit voltage (V_{oc}) and 4% higher fill factor. Resulting in a higher device performance with $MAPbI_3$ [m] perovskite particles. The incident photon to electron conversion efficiency (IPCE) of the perovskite devices is illustrated in Fig. 4b. The IPCE of the reference device is slightly higher compared to the device prepared with $MAPbI_3$[m] sample in line with the observed 1 mA/cm^2 higher current density. The onsets of IPCE spectra of both the devices are very similar.

We also measured the hysteresis of both the devices by recording current-voltage characteristics at 100 mV/sec sweep rate, starting with a backward scan and directly continuing with a forward scan as shown in Fig. 5. It is interesting to observe that devices made from $MAPbI_3$[m] perovskite particles shows almost no hysteresis, while for the $MAPbI_3$[s] cell it produces a 1.5 % lower efficiency. Recently the origin of hysteresis in perovskite solar cells has been widely discussed and suggested that this phenomenon is due to ferroelectric, polarization or trap state filling effects.[6,27,28] It is also suggested that the presence of defect states to be a crucial factor in determining anomalous hysteresis in perovskite solar cells. Therefore significant improvements of crystal quality allowing for

View Article Online
DOI: 10.1039/C5TA04904K

hysteresis-free perovskite solar cells have been achieved after introducing several new crystal growth methods.[28,29] The favourable outcome of the mechanosynthesis undoubtedly highlights its exceptional quality in obtaining perovskite with low defect levels.
Based on this we believe that hysteresis in perovskite solar cells fabricated with mechanosyntheticaly prepared perovskite particles is also reduced due to the presence of the lower amount of defects in particular electron or hole traps. Moreover, mechanochemistry provide $MAPbI_3$ perovskite particles showing exact stoichiometric composition what can additionally results to both lower hysteresis and better PCE in comparison to that synthesized by using one-step process. Higher purity of material could contribute to better power conversion efficiencies for devices obtained using this new synthesis method.

Table 1 Photovoltaic characteristics[a] of cells measured under illumination with standard AM 1.5G simulated sunlight (100 mW/cm^2)

Device	Eff. (%)	FF	V_{oc} (mV)	J_{sc} (mA cm^{-2})
$MAPbI_3$[s]	8.0±0.2	68±0.8	778±5.9	15.2±2.9
	(8.2)	(68)	(777)	(15.1)
$MAPbI_3$[m]	8.9±0.2	72±0.9	878±7.8	14.2±1.6
	(9.1)	(72)	(879)	(14.1)

[a] The average data with standard deviation were based on few identical cells (see T2 in SI); the data for the best performing cells are given in parentheses.

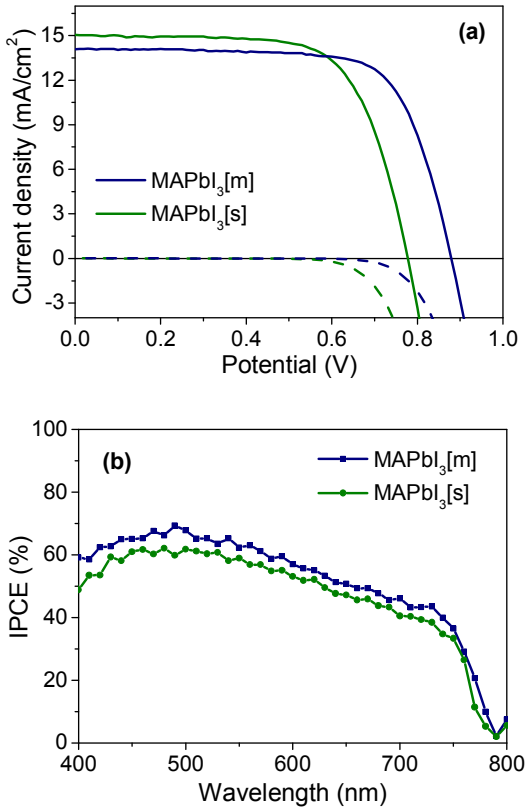

Figure 4 Current-voltage characteristics (a) and IPCE (b) of the perovskite MAPbI3[s] solar cell (green) and cell made with $MAPbI_3$[m] particles (blue).

It remains to be explained why the mechano-synthesized perovskite performs better than the one prepared using the one-step solution process. We note that there is an important difference between the perovskite film prepared via the mechano-chemical synthesis route and films made by the one step solution process. The mechano-chemical route produces the $MAPbI_3$ perovskite material first in pure crystalline form as shown by the full characterization of the material described above. The subsequent deposition of the thin film perovskite on the mesoscopic TiO_2 scaffold to fabricate the photovoltaic device amounts to recrystallization of the powder from DMF as a solvent, which likely will result in further purification. In contrast to the mechano-chemically synthesized $MAPbI_3$ perovskite it is difficult to prepare films of exact stoichiometric composition by the one step solution method. While one aims for making a starting solution containing the PbI_2 and CH_3NH_3I in a 1:1 molar ratio the weighing in of the precursors is not precise enough to avoid a slight deviations from the desired stoichiometry. This results in the formation of lattice defects, which often affect adversely the photovoltaic performance of the perovskite. Thus, an excess of methyl-ammonium iodide will create lead ion vacancies that can act as electron traps and accelerate the radiation-less recombination of charge carriers lowering the open circuit voltage of the device and hence its power conversion efficiency. This rational is supported by previous investigations showing that excess halides in the perovskite induce defects.[30,31]

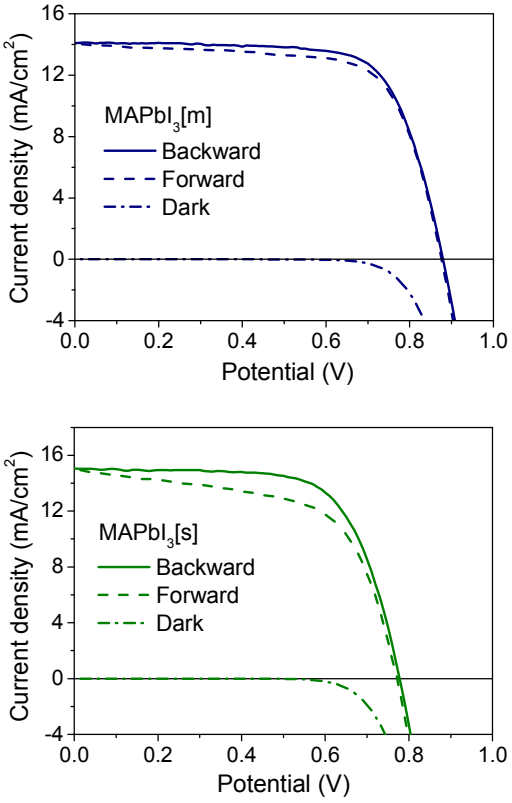

Figure 5. Current-voltage curves of devices prepared with standard MAPbI3[s] perovskite and $MAPbI_3$[m] perovskite to study the hysteresis effect. Scan rate 100 mV/sec.

Conclusions

In conclusion, we presented mechanosynthesis as a new an alternative chemical approach that allows us to obtain $MAPbI_3$

View Article Online
DOI: 10.1039/C5TA04904K

perovskite particles showing of exact stoichiometric composition and high thermal stability. X-ray diffraction studies confirmed no detectable amounts of starting materials. In addition, newly synthesized perovskite material gave superior device performance compared to standard solution processed synthesis which opens up a new avenue for making cheap and highly performed perovskite materials for solar cell applications without hysteresis.

Experimental

Materials synthesis

Polycrystalline methylammonium iodide perovskite particles were obtained by applying mechanochemical processing technique. To this end, lead iodide (PbI_2) (99,999% Pb) ABCR) (461 mg; 1 mmol) and methylammonium iodide (MAI) (DYESOL) (159 mg; 1 mmol) were mixed together in a 10 mL agat jar with one 10 mm diameter agat ball. The mixture was ground for 30 min in a Retsch MM200 mill at 30 Hz yielding a black polycrystalline material. The synthesis was conducted in glove box under an argon atmosphere.

Solar cell device fabrication

Devices were prepared on plasma-cleaned conductive fluorine-doped tin oxide (FTO) coated glass substrates. A compact 50 nm thick titanium dioxide layer was deposited by spray pyrolysis of 9 ml ethanol solution containing 0.6mL titanium diiso-propoxide bis(acetylacetonate) solution (75% in 2-propanol, Sigma-Aldrich) and 0.4mL acetylacetone at 450° C in air. On top of this compact layer, a 300 nm-thick mesoporous titanium dioxide layer was prepared by spin-coating 30 nm sized nanoparticles (Dyesol 30NRD, Dyesol) diluted in ethanol (1:3.5 wt/wt) at 4800 rpm for 30 s. The films were then gradually heated to 500 °C and sintered at that temperature for 1.5 h under oxygen at-mosphere. Perovskite stock solution in N,N-dimethylformamide was prepared from lead iodide (PbI_2) of 1.2M concentration by mixing it with methylammonium iodide in molar ration 1:1.05 by vigorous stirring at 130° C. The stock solution of mechanosynthesis lead io-dide perovskite particles was prepared by dissolving them in N,N-dimethylformamide (2:5 wt/wt) by vigorous stirring at 130 °C. Prepared stock solutions were spin coated on top of the mesoporous TiO_2 layer at 6500 rpm for 20 s and dried at 70 °C degrees for 15 min to form perovskite films. Hole transporting material (HTM) solution was prepared by dissolving 74 mg spiro-MeOTAD in 1 ml chlorobenzene and additionally mixing it with 17.5 µL of lithium bis(trifluoromethylsulphonyl)imide (stock solution Li-TFSI 520 mg·mL^{-1} in acetonitrile), 28.8 µL tert-butylpyridine and 29 µl of tris(2-(1H-pyrazol-1-yl)-4-tert-butylpyridine)cobalt(III) bis(trifluoromethylsulphonyl) imide (stock solution FK 209, 300 mg·ml^{-1} in acetoni-trile). Subsequently, HTM was deposited on top of the perovskite layer by spin coating at 3000 rpm for 20 s. Device fabrication was completed by thermal evaporation of 60 nm thick gold layer on top of the pure perovskite and perovskite with HTM. The active area of the devices is approximately 0.56 cm^2.

Device characterization

Current voltage characterization

The *J-V* characteristics of the devices were measured under 100 mW/cm^2 conditions using a 450 W Xenon lamp (Oriel), as a light source, equipped with a Schott K113 Tempax sunlight filter (Praezisions Glas & Optik GmbH) to match the emission spectra to the AM1.5G standard in the region of 350-750 nm. The current–voltage characteristics of the devices were obtained by applying external potential bias to the cell while recording the generated photocurrent using a Keithley (Model 2400) digital source meter. The *J-V* curves of all devices were measured by masking the active area with a metal mask of area 0.16 cm^2.

Internal photon to current conversion efficiency

The internal photon to current conversion efficiency of the devices was measured by focusing light from the 300W Xenon lamp (ILC Technology, U.S.A.) through a Gemini-180 double monochromator (Jobin Yvon Ltd., U.K.) while chopping at 3 Hz before illuminating onto the photovoltaic cell. The monochromator was incremented through the visible spectrum to generate the IPCE dependence on wavelength.

Techniques

Powder X-Ray diffraction

Powder XRD data were collected on Empyrean diffractometer (PANalytical). Measurements employed Ni-filtered Cu Kα radiation of a copper sealed tube charged with 40 kV voltage and 40 mA current and Bragg-Brentano geometry with beam divergence of 1 deg. in the scattering plane. Diffraction patterns were measured in the range of 4-50 degrees of scattering angle by step scanning with step of 0.02 degree.

Thermogravimetric analysis

Thermogravimetric analysis (TGA) was performed on TA Instruments Q600 system at a heating rate of 50°C·min^{-1} from 25 to 600°C under argon atmosphere. Such a slow heating rate was used in order to accurately determine full sample decomposition at the corresponding temperature.

Structure characterization

The surface morphology of the perovskite was explored by a Nova 450 NonoSEM scanning electron microscope (SEM) with energy resolution of 130 eV.

Energy Dispersive X-Ray Analysis. The elemental compositions of the samples were determined using the energy dispersive X-ray fluorescence (EDXRF) spectrometer (MiniPal 4, PANalytical&Co) with Rh tube and silicon drift detector. The spectra were collected in air atmosphere, without using a filter, at a tube voltage of 20 kV. The time of acquisition was set to 50 s and the tube current up to 50 µA.

Optical measurements. Ultraviolet–visible diffuse reflec-tance spectroscopy was performed using a UV-2501PC Shimadzu

View Article Online
DOI: 10.1039/C5TA04904K

spectrophotometer in the 250-900 nm spectral range. Fluorescence decay kinetics were recorded with spectrofluorometer Fluorolog 322 working in single-photon counting mode. Picosecond pulsed diode laser head NanoLED-405LH (Horiba) emitting <200 ps duration pulses at 406 nm with repetition rate of 1 MHz was used for sample excitation. The excitation energy was about 11 pJ/pulse. Fluorescence spectrum was corrected for the instrument response function. The maximum reached time resolution of the setup was about several hundred picoseconds by applying apparatus function deconvolution.

Acknowledgements

M.G. acknowledges financial support from a Sciex fellowship under Project Code 13.194, CCEM-CH in the 9th call proposal 906: CONNECT PV, Swiss National Science Foundation (SNF)-NRP70 (PV2050, 407040-153990 and 40740-153952) and J.L. acknowledges support of FNP Program "Mistrz".

Notes and references

1 W. S. Yang, J. H. Noh, N. J. Jeon, Y. C. Kim, S. Ryu, J. Seo and S. I. Seok, *Science*, 2015, **348**, 1234.
2 L. Zheng, Y. Ma, S. Chu, S. Wang, B. Qu, L. Xiao, Z. Chen, Q. Gong, Z. Wuc and X. Hou, *Nanoscale*, 2014, **6**, 8171.
3 S. D. Stranks, G. E. Eperon, G. Grancini, C. Menelaou, M. J. P. Alcocer, T. Leijtens, L. M. Herz, A. Petrozza and H. J. Snaith, *Science*, 2013, **342**, 341.
4 deQuilettes, D. W. et al. *Science,* 2015, **348**, 683.
5 C. Wehrenfennig, G. E. Eperon, M. B. Johnston, H. J. Snaith and L. M. Herz, *Adv. Mater.,* 2014, **26**, 1584.
6 J. Snaith, A. Abate, J. M. Ball, G. E. Eperon, T. Leijtens, N. K. Noel, S. D. Stranks, J. T. -W. Wang, K. Wojciechowski and W. Zhang, *J. Phys. Chem. Lett.*, 2014, **5**, 1511.
7 A. Ecija, A. Larrañaga, K. Vidal, L. Ortega and M. I. Arriortua, in *Advances in Crystallization Processes*, ed. Y. Mastai, InTech, 2012, pp. 485-506.
8 Q. Dong, Y. Fang, Y. Shao, P. Mulligan, J. Qiu, L. Cao and J. Huang, *Science*, 2015, **347**, 967.
9 K. Wang, C. Liu, P. Du, H. –L. Zhang and X. Gong, *Small*, 2015, DOI: 10.1002/smll.201403399.
10 T. Baikie, Y. Fang, J. M. Kadro, M. Schreyer, F. Wei, S. G. Mhaisalkar, M. Graetzel and T. J. White, *J. Mater. Chem. A*, 2013, **1**, 5628.
11 C. C. Stoumpos, C. D. Malliakas and M. G. Kanatzidis, *Inorg. Chem*., 2013, **52**, 9019.
12 J. Lewiński, M. Dutkiewicz, M. Lesiuk, W. Śliwiński, K. Zelga, I. Justyniak and J. Lipkowski, *Angew. Chem. Int. Ed*., 2010, **122**, 8442.
13 D. Prochowicz, I. Justyniak, A. Kornowicz, S. Komorski and J. A. Lewiński, *Inorg. Chem. Commun*., 2014, **46**, 216.
14 D. Prochowicz, K. Sokołowski, I. Justyniak, A. Kornowicz, D. Fairen-Jimenez, T. Friščić and J. Lewiński, *Chem. Commun*., 2015, **51**, 4032.
15 D. Prochowicz, I. Justyniak, A. Kornowicz, T. Kaczorowski, Z. Kaszkur and J. Lewiński, *Chem. Eur. J*., 2012, **18**, 7367.
16 J. –H. Im, C. –R. Lee, J. –W. Lee, S. –W. Park and N. –G. Park, *Nanoscale*, 2011, **3**, 4088-4093.
17 J. Burschka, N. Pellet, S. –J. Moon, R. Humphry-Baker, P. Gao, M. K. Nazeeruddin and M. Grätzel, 2013, **499**, 316.
18 Q. Chen, H. Zhou, Z. Hong, S. Luo, H.-S. Duan, H. -H. Wang, Y. Liu, G. Li and Y. Yang, *J. Am. Chem. Soc*., 2014, **136**, 622.
19 C. –W. Chen, H. –W. Kang, S. –Y. Hsiao, P. –F. Yang, K. –M. Chiang and H. –W. Lin, *Adv. Mater*., 2014, **26**, 6647.
20 M. Liu, M. B. Johnston and H. J. Snaith, *Nature*, 2013, **501**, 395.
21 K. Liang, D. B. Mitzi and M. T. Prikas, *Chem. Mater*., 1998, **10**, 403.
22 Y. Kawamura, H. Mashiyama and K. Hasebe, *J. Phys. Soc. Jpn*., 2002, 71, 1694.
23 A. Dualeh, P. Gao, S. I. Seok, M. K. Nazeeruddin and M. Grätzel, *Chem. Mater*. 2014, **26**, 6160.
24 A. M. A. Leguy, Y. Hu, M. Campoy-Quiles, M. I. Alonso, O. J. Weber, P. Azarhoosh, M. van Schilfgaarde, M. T. Weller, T. Bein, J. Nelson, P. Docampo and P. R. F. Barnes, *Chem. Mater*. 2015, **27**, 3397.
25 C. Pélégris, M. Rivenet, M. Traisnel, In *Fire Retardant Fillers for Polymers: New Applications of Mineral Fillers*, eds. M. L. Bras, C. A. Wilkie, S. Bourbigot, S. Duquesne, C. Jama, RSC, Cambridge, United Kingdom, 2005; pp 68-78.
26 W. Xie, Z. Gao, W. –P. Pan, D. Hunter, A. Singh and R. Vaia, *Chem. Mater*., 2001, **13**, 2979.
27 W. Tress, N. Marinova, T. Moehl, S. M. Zakeeruddin, M. K. Nazeeruddin and M. Grätzel, *Energy Environ. Sci.*, 2015, **8**, 995.
28 D. Shi, V. Adinolfi, R. Comin, M. Yuan, E. Alarousu, A. Buin, Y. Chen, S. Hoogland, A. Rothenberger, K. Katsiev, Y. Losovyj, X. Zhang, P. A. Dowben, O. F. Mohammed, E. H. Sargent and O. M. Bakr, *Science*, 2015, **347**, 519.
29 W. Nie, H. Tsai, R Asadpour, J. -C. Blancon, A. J. Neukirch, G. Gupta, J. J. Crochet, M. Chhowalla, S. Tretiak, M. A. Alam, H. –L. Wang and A. D. Mohite, *Science*, 2015, **347**, 522.
30 A. Buin, R. Comin, J. Xu, A. H. Ip and E. H. Sargent, *Chem. Mater*., 2015, **27**, 4405.
31 A. Buin, P. Pietsch, J. Xu, O. Voznyy, A. H. Ip, R. Comin and E. H. Sargent, *Nano Lett*., 2014, **14**, 6281.